analytical chemistry

pubs.acs.org/ac Article

Embracing Poisson Encapsulation Statistics for Improved Droplet Digital Immunoassay

Yujuan Chai, Xiaoxiang Hu, Qi Fang, Yuanyuan Guo, Binmao Zhang, Hangjia Tu, and Zida Li*

Cite This: *Anal. Chem.* 2025, 97, 444−453 Read Online

ACCESS | Metrics & More | Article Recommendations | Supporting Information

ABSTRACT: Digital immunoassays enable the detection of protein biomarkers with very low concentrations, but the analysis stringently requires single-bead encapsulation. Low bead density has been adopted to minimize multiple-bead encapsulations, but the trade-off is the low droplet effectiveness (∼10%) in droplet-based assays. Here we report the method of inclusive droplet digital ELISA (iddELISA) that embraces all types of encapsulations by factoring in their varied "on−off" probabilities in the statistical inference. We derived the statistical model, optimized the bead encapsulation and immunoreaction, and developed an image analysis pipeline for accurate droplet and bead recognition, showing that approximately 40% of the droplets could be used in the analysis. Using the detection of SARS-CoV-2 nucleocapsid protein as a demonstration, the iddELISA achieved a limit of detection of 0.71 fg/mL, which was much lower than conventional ELISA as well as droplet digital ELISA. By effectively incorporating multiple bead encapsulations, the iddELISA simplified the digital immunoassay while improving the counting efficiency and sensitivity, representing a unique concept in digital immunoassays.

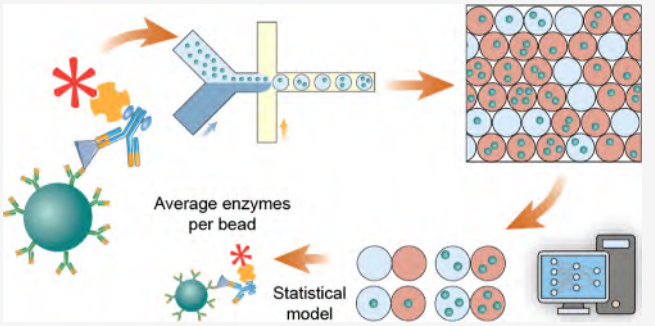

INTRODUCTION

Accurate and sensitive detection of biomarkers plays an important role in clinical diagnosis and basic research.[1,2] Such detection has been commonly achieved by immunoassays such as enzyme-linked immunosorbent assay (ELISA), chemiluminescent immunoassay, and lateral flow assay based on the specific antigen−antibody binding and formation of immunocomplex that generates test signals.[3] However, these assays fall short in accuracy and detection limit when analytes of ultralow concentrations are examined.

Digital immunoassays provide detection strategies with better sensitivity and quantification capability. For example, nanoparticles have been proposed as the medium to capture or visualize analytes. Using sophisticated technologies such as surface plasmon resonance,[4,5] and solid-state nanopores,[6] the analyte concentrations can be calculated by digital counting of the nanoparticles and signals. Despite the improved performance in analyte quantification, the assay sensitivity of these nanoparticle-based assays is still inadequate.

Digital ELISA can detect proteins at the femtogram-picogram level.[7] The enzyme-linked immuno complexes are formed on beads and distributed into thousands of compartments, confining the catalytic products (usually fluorescent) into individual chambers to enhance the signals. The signals of each compartment are detected and binarized, and the percentage of positive compartments is used to infer the analyte concentration. Bead compartmentalization has been implemented using microwells with demonstrated success.[8] For example, such assays have been applied for early detection of cytokine release syndromes in patients with COVID-19.[9] Nevertheless, high-efficiency bead loading into the microwells is not trivial, and the bead reading is prone to error.[10] In addition, the number of microwells is limited by the chip size, making it difficult to scale up.

Microfluidics can generate uniform droplets with high throughput, providing an alternative means to bead compartmentalization and analysis.[11] Indeed, droplets have been utilized in lieu of microwells in the implementation of droplet digital ELISA (ddELISA).[12] However, during droplet generation, the bead encapsulation is dictated by the Poisson distribution: a certain portion of the generated droplets would contain more than one bead, which alters the specific probability distribution of "on"−"off" status of individual droplets, making the analysis less accurate. Low bead densities are commonly used to minimize multiple bead encapsulation, but it also brings about large amount of undesirable empty droplets (>90%). Though inertial focusing has been adopted to beat the Poisson encapsulation statistics and increase the

Received: August 26, 2024
Revised: November 8, 2024
Accepted: November 12, 2024
Published: November 18, 2024

https://doi.org/10.1021/acs.analchem.4c04552
Anal. Chem. 2025, 97, 444−453

percentage of single-bead encapsulations, the performance was sensitive to flow conditions and bead sizes, making it difficult to apply in practice.[13,14] Hydrogel coating has been proposed to increase the efficiency of single-bead encapsulation through close-packed ordering, but the coating inevitably masks the capture antibody coated on the beads.[15] ddELISA technologies with convenient bead manipulation are yet to be developed.

Instead of excluding the multiple bead encapsulations, here we report the method of inclusive droplet digital ELISA (iddELISA) that embraces all types of encapsulations. iddELISA uses relatively high bead density for droplet generation, resulting in about 40% droplets containing one, two, or more beads. In the analysis, the "on−off" status of each droplet as well as the number of beads encapsulated within are used in conjunction to infer the analyte concentration based on the Poisson distribution. We derived the statistical model, optimized the bead encapsulation and immunoreactions using SARS-CoV-2 nucleocapsid (N) protein as the analyte, and developed the image analysis pipeline for droplet and bead detection using deep learning. As a result, the iddELISA achieved a limit of detection as low as 0.71 fg/mL (15.78 aM) with a coefficient of variation (CV) of less than 12.73% during performance characterization. In comparison, convential ELISA and standard ddELISA had LODs of 4.12 pg/mL and 7.01 fg/mL, respectively, using the same reagents, underscoring the enhanced capability of iddELISA for ultra-sensitive detection. By incorporating multiple bead encapsulations into the analysis, iddELISA represents a unique concept in digital immunoassays, offering simplified operation and improved sensitivity.

METHODS

Reagents and Materials. Details of the reagents and materials are listed in Table S1. Reagents and materials used for microfluidic chip fabrication and droplet generation include polydimethylsiloxane (PDMS), Trichloro (1*H*,1*H*,2*H*,2*H*-perfluorooctyl) silane, droplet generation oil, and 3 M Novec 7500. Reagents and materials used in the immunoassays are SARS-CoV-2 N protein (2.35 mg/mL), capture antibody (7.35 mg/mL), detection antibody (7.09 mg/mL), 10 μm magnetic beads (32 k/μL), and EZ-Link NHS-PEG12-Biotin. The enzymes and substrate for fluorescent signal generation are streptavidin-conjugated HRP (1 mg/mL), streptavidin-conjugated Poly-HRP (1 mg/mL), streptavidin-conjugated high sensitivity-HRP (SA HS-HRP, 1 mg/mL) and Amplite red. *N*-(3-Dimethylaminopropyl)-*N*′-ethylcarbodiimide hydrochloride (EDC·HCl) and sulfo *N*-hydroxysuccinimide (Sulfo·NHS) are used for capture antibody conjugation to the beads. Other reagents applied as blocking agents or buffer components are blocker casein in phosphate buffer saline (PBS), Tween 20, polyethylene glycol 8000 (PEG 8000), bovine serum albumin (BSA), casein, PBS, Dulbecco PBS (DPBS), sodium tetraborate decahydrate ($Na_2B_4O_7$, $10H_2O$), boric acid (H_3BO_3), sodium hydroxide (NaOH), and ethanolamine (C_2H_7NO).

Preparation of the Beads and Detection Antibody. Conjugation of the capture antibody to the 10 μm COOH nodified MBs (Vdo Biotech) was performed with a typical EDC/NHS-based reaction. Briefly, 50 μL MBs were washed three times with PBST buffer (pH = 7.3, 0.01% Tween20) and resuspended in 250 μL of activation buffer (5 mM boric acid-saline buffer, pH = 7.2, 0.01% Tween20). Then, 16.67 μL of EDC·HCl (75.6 mg/mL) and Sulfo·NHS (54 mg/mL) were added to the beads and sonicated for 5 min before washing and resuspended in 250 μL coupling buffer (5 mM borate buffer solution, pH = 8.0, 0.01% Tween20). To investigate the appropriate amount of capture antibody, four different volumes of capture antibody (10, 20, 30, and 40 μL, mAb17) were added to the beads and incubated overnight at 4 °C. After the reaction, 16.67 μL of 10% casein and 0.8 μL of ethanolamine were added to the solution and incubated for 30 min at 37 °C with rotation. The beads were washed three times with coupling buffer and once with PBST buffer, and resuspended in 500 μL incubation buffer (1× PBS, pH = 7.3, 1% BSA, 0.1% PEG8000, 0.01% Tween20) overnight at 4 °C. Finally, the beads were washed three times with PBST and dispersed in 50 μL of storage buffer (1× PBS, pH = 7.3, 0.1% BSA, 0.05% Tween20) for further use. Optimization of the amount of capture antibodies was conducted with standard immunofluorescent assays as described in our previous study.[24] Briefly, 10 μL conjugated MBs were mixed with 50 μL PBS buffer and 50 μL N protein antigen (0 or 100 ng/mL, Ag_6), followed by the addition of detection antibody (0.9 μg/mL, mAb15) conjugated with fluorescent molecules. The conjugation of antibodies with fluorescent molecules was consistent with the conjugation protocol of the capture antibody to the MBs. The fluorescent molecules were quantum dots (QDs) synthesized by our lab. After rotating incubation at 37 °C for 30 min, the immuno complex was washed with 200 μL PBST buffer three times. The fluorescence images of the beads were captured under a fluorescence microscope, and the signal intensity was analyzed using ImageJ. Each experiment was repeated three times.

To construct the detection probe for iddESLIA, the detection antibody was first diluted in DPBS to 2 mg/mL for biotin conjugation. Then, 1.41 μL of 50 mM NHS-PEG12-Biotin was mixed with 53 μL antibody, shaking at room temperature for 30 min before being stored at 4 °C for future use. The molar ratio of biotin to detection antibody and the concentration of biotinylated detection antibody were optimized with iddELISA. For the biotin-to-detection antibody ratio optimization, three different molar ratios (5:1, 10:1, and 20:1) at three antigen concentrations (0, 500, and 2500 fg/mL) were tested. Similarly, for the evaluation of the detection antibody concentration, four different conditions (20, 100, 400, 800 ng/mL) at the same three antigen concentrations (0, 500, and 2500 fg/mL) were tested. The standard iddELISA as described in the following section was performed for each experimental condition.

Design and Fabrication of Microfluidic Devices. Two microfluidic devices were used: one for droplet generation and one for droplet observation, as shown in Figure S1a−c. The droplet generation chip had three inlets for the oil phase, bead suspension, and the substrates, respectively, and one outlet for droplet collection. The smallest feature of the channel at the cross-junction was 30 μm, and the height of the channel was 50 μm. The observation chip had one inlet and one outlet. The overall dimensions of the chamber were 0.5 × 2 cm, and the height of the chamber was 45 μm. Each chamber can accommodate approximately 12.5k droplets with diameters of 50 μm.

The microfluidic devices were fabricated by replicating the patterns of SU-8 photoresist on silicon wafers using PDMS. Fabrication of the SU-8 molds was outsourced to a microfabrication company (Suzhou Research Materials Microtech Company, China). The fabricated SU-8 molds were

https://doi.org/10.1021/acs.analchem.4c04552
Anal. Chem. 2025, 97, 444−453

treated with a plasma cleaner for 2 min, then placed in a vacuum chamber for 5−6 h where it was exposed to silane vapor. The PDMS was mixed with the curing agent in a ratio of 10:1. After degassing, the mixture was poured onto the SU-8 mold and heated for at least 6 h at 65 °C. Then, the PDMS sheets were cut and peeled from the mold and punched with a 1.1 mm puncher for the generation of Finlets and outlets. After plasma treatment for 1 min, the PDMS chips were placed on a clean cover glass and heated at 110 °C for 1 h for secure bonding.

iddELISA. The SARS-CoV-2 N protein was diluted with reaction buffer (1× PBS, pH 7.30, 0.1% casein, 0.01% Tween20) or 10% artificial saliva buffer (10% artificial saliva and 90% reaction buffer) to the desired concentration (0, 2, 4, 20, 100, 500, 2500, and 12500 fg/mL). The former represents a typical "clean" matrix whereas the latter mimics the matrix of swab samples commonly used for SARS-Cov-2 sampling.[24,25] A total of 80k beads (2.5 μL) were used for each iddELISA assay. The beads were mixed with 100 μL antigen solution and 100 μL of 400 ng/mL biotinylated detection antibody, and incubated at 37 °C on a rotating incubator (MX-RL-E, DLab Scientific) for 30 min. The beads were then collected with a magnet and washed 3 times with PBST before 200 μL of SA−HS−HRP was added. The mixture was incubated at 37 °C in a rotating incubator for 10 min, followed by the collection of immunomagnetic beads. After washing for another 4 times, the beads were resuspended in 10 μL of PBS buffer and vortexed for at least 30 s.

The substrate solution was prepared by mixing 1.5 μL 100 mM H_2O_2 and 155 μL 16× Amplite Red solution. Two syringes connected with tubing were used to draw up the beads and the substrate solutions into the tubing, respectively, to minimize the dead volume upon infusing. Syringe pumps were then used to inject the beads and substrate into the droplet generation chip. The flow rates of the aqueous phases were both 240 μL/h, and the flow rate of the oil phase was 1200 μL/h. The chip was observed using a microscope (Eclipse Ts2, Nikon) to monitor the droplet generation process using a high-speed camera (VEO E-310 L, Phantom). Once the droplet generation stabilized, a pipet tip was inserted into the outlet to collect the droplets for 2.5 min. The droplets were then transferred to an Eppendorf tube and incubated for approximately 6 min in the dark. Droplet generation oil was used to flush the observation chip before the droplets were loaded into the observation chamber. Both brightfield and fluorescence micrographs were acquired using a fluorescence microscope (Eclipse Ti2-E, Nikon) coupled with a camera (DS-Qi2, Nikon). The total imaging time was about 4 min. In practice, 6 reactions can be handled in parallel and the droplet generation/imaging steps can be performed one assay after another. All assays described in this study are single-plexed, with the equipment shown in Figure S1b−f.

When studying the effects of flow rates on droplet sizes, the oil phase was fixed at 1200 μL/h, and the two aqueous had the same flow rates, with 150, 200, 240, and 300 μL/h tested. The droplets were then collected and loaded into the observation chip for brightfield imaging. The droplet sizes were analyzed in ImageJ. When studying the dispersion volume of the beads, 80k beads were dispersed into 10, 12.5, 15, and 20 μL PBS solution for droplet encapsulation. The flow rates of the oil and both aqueous phases were 1200 and 240 μL/h, respectively. The droplets were imaged in the observation chip and analyzed in Python. When studying the bead numbers, 50, 60, 70, 80, 90, and 100k beads were dispersed in 10 μL PBS solution to perform the droplet encapsulation, before being analyzed similarly. When comparing the performance of different streptavidin conjugated enzymes, namely HRP, HS-HRP, and Poly-HRP, the enzyme with concentrations of 12.5 ng/mL was used as an aqueous phase, and 16× Amplite red substrate was used as the other aqueous phase for droplet generation. The droplets were then loaded into the observation chip for fluorescence imaging at 10, 20, and 30 min after the droplet formation. The fluorescence intensity was analyzed using ImageJ.

Conventional ELISA. The ELISA experiment was performed using a standard 96-well plate. First, 100 μL of 2 μg/mL capture antibody was dispensed into each well and incubated overnight at room temperature. Afterward, 300 μL of BSA buffer (1× PBS, pH 7.30, 1% BSA) was added to each well for 1 h blocking, followed by three washing steps with 300 μL 1× PBS. The antigen samples were prepared by diluting the SARS-CoV-2 N protein in BSA buffer to the specified concentrations (1000, 500, 250, 125, 62.5, 31.3, 15.6, 7.81, 3.91, 1.95, 0.98 pg/mL). For each assay, 100 μL of antigen sample was added and incubated at room temperature for 2 h. Then, 100 μL of 500 ng/mL capture antibody was added for another 2 h incubation at room temperature, followed by the addition of 100 μL SA-HS-HRP and 20 min of incubation. Finally, 100 μL of TMB was introduced for a light-protected incubation of 6 min before the measurement with an enzyme-linked immunosorbent assay reader. Between each incubation step, the wells were washed three times with 300 μL of PBST buffer. Each experiment was repeated in triplicate, and 4-parameter logistic fit was applied to calculate the LOD and LOQ (Figure S7).

ddELISA. The procedure and reagent concentrations of the ddELISA were consistent with those of the iddELISA. However, after completing the immunoreaction and attaching the SA−HS−HRP, the magnetic beads were resuspended in 20 μL PBS, followed by droplet generation and image capture. The same algorithm and model were employed for image analysis, but focused exclusively on the single-bead droplets (like the standard ddELISA) for the calculation of the AEB (using Poisson distribution). Each experiment was repeated in triplicate, and the calculation of LOD and LOQ was consistent with the conventional ELISA and iddELISA (Figure S8).

Image Analysis and Data Analysis. The image analysis pipeline was developed in Python and mainly included three tasks, namely the detection of droplets, the detection of beads, and analysis of the droplet fluorescence. The detection of droplets and beads was achieved by implementing the deep learning algorithm of YOLOv5.[21] The algorithm employed focus and CSP-darknet as the backbone layer, FPN and PAN as the neck layer, and CIOU loss as the loss function in the head layer. The original image was sliced into four parts in the focus layer, which were then concatenated and passed through a convolutional layer. The network included components such as CBL, CSP1-x, CSP2-x, and SPP, which consisted of convolution, batch normalization, leaky ReLU, cross stage partial networks, and spatial pyramid pooling, respectively. This design enabled the algorithm to extract meaningful features, capture complex relationships, and produce accurate bounding box predictions. Also, YOLOv5 as a single-stage object detection model, offers faster processing speeds, lower resource requirements, and simpler implementation, which is suitable for our iddELISA system.

https://doi.org/10.1021/acs.analchem.4c04552
Anal. Chem. 2025, 97, 444−453

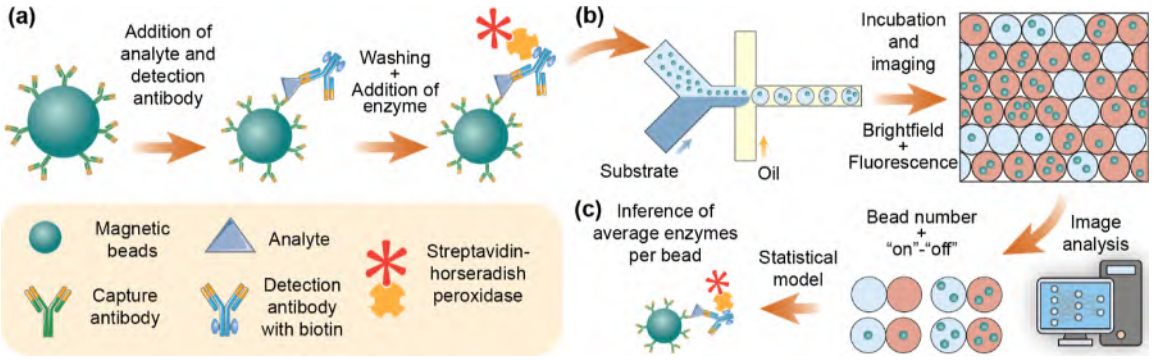

Figure 1. Principle of the inclusive droplet digital ELISA (iddELISA). Droplets containing multiple beads are also observed to infer the average enzymes per bead. (a) Generation of the immunocomplex on beads. (b) Encapsulation of beads into droplets and the subsequent imaging. (c) Image and data analysis. Both the "on−off" status and bead numbers of the droplets are analyzed.

The data sets were annotated in LabelImg.[26] The droplet data set contained more than 27 thousand droplets from 60 brightfield images, and the bead data set contained over 500 beads from 350 droplets. The data sets were split at training-test ratios of 2:1 and 3:1 for droplets and beads, respectively. The models were trained for 300 epochs and 50 epochs for droplets and beads, respectively, on a GPU (GeForce RTX 3080 Ti, Nvidia Corporation). The detected droplets were filtered to keep droplets with aspect ratios between 0.85 and 1.5 and sizes between 75 and 130 pixels (45−78 μm). This additional operation removed the incomplete droplets straddling the image edges and those with abnormal size.

Droplet fluorescence was analyzed by mapping the bounding boxes in the brightfield images to the fluorescence counterparts. The bounding boxes were then scaled to 1/8 to the center to compensate for the droplet shifting during imaging. The average fluorescence intensities within the bounding boxes were then calculated. Droplets containing no beads served as the internal references of "off" droplets, and the mean plus five standard deviations of their fluorescence intensities were used as the cutoff threshold between "on" and "off" droplets. Together, the bead numbers and the "on"−"off" status of each droplet were obtained. These data were then compiled and used to calculate the average enzymes per bead by solving eq 6 and then eq 1.

When evaluating the analytical performance, samples with analyte concentrations of 0, 2, 4, 20, 100, 500, 2500, and 12,500 fg/mL were tested three times. The AEBs were calculated, and the data was fitted with a four-parameter logistic model (Origin, OriginLab). The limit of detection and the limit of quantification were calculated as the mean AEBs of blank samples plus three or ten standard deviations, respectively. All LOD and LOQ refer to the concentrations of the samples to be tested. To assess the repeatability of the iddELISA assay, three concentrations of the analyte (20, 100, and 2500 fg/mL) were tested in six replicates. The coefficients of variation were calculated as the standard deviation divided by the mean. The recovery rates were calculated as the mean of measurements divided by the spiked concentration.

RESULTS

Overview of the Inclusive Droplet Digital ELISA. The iddELISA includes all types of bead encapsulations in the analysis by considering the varied probabilities of individual droplets being "on". Similar concepts were adopted in digital nucleic acid tests using polydisperse droplets by us and others.[16,17] After the formation of immuno complexes on the beads, the probability of a specific bead containing at least one enzyme, q, follows the Poisson distribution that

$$q = 1 - e^{-\lambda} \tag{1}$$

where λ is the average enzymes per beads (AEB). Consequently, the probabilities of a droplet with i bead(s) being "on" and "off", denoted as $P_{i,+}$ and $P_{i,-}$, respectively, are

$$P_{i,+} = 1 - (1 - q)^i \tag{2}$$

$$P_{i,-} = (1 - q)^i \tag{3}$$

In a given experimental observation, assuming the numbers of "on" and "off" droplets containing i bead(s) are n_i and m_i, respectively, the likelihood function is

$$L(\lambda; n_i, m_i) = \prod_{i=1}^{\infty} P_{i,+}{}^{n_i} \cdot P_{i,-}{}^{m_i} \tag{4}$$

The value of the parameter, λ, that maximizes the likelihood function is considered the most probable value of the AEB, is

$$\hat{\lambda} = \arg\max_{\lambda \in (0,1)} \ln L(\lambda; n_i, m_i) \tag{5}$$

The natural logarithm is applied to the likelihood function for the convenience of calculation. In practice, since the droplets containing four or more beads account for less than 1.6% of the bead-containing droplets, we treated droplets containing three or more as a group and used $P_{3,+}$ and $P_{3,-}$ to describe all droplets in this group to allow easier equation solving (see Supporting information note). Consequently, the most probable q can be found by solving

$$\frac{n_1}{1-(1-q)} + \frac{2n_2(1-q)}{1-(1-q)^2} + \frac{3n_3'(1-q)^2}{1-(1-q)^3} - \frac{m_1 + 2m_2 + 3m_3'}{1-q} = 0 \tag{6}$$

where n_3' and m_3' represent the total numbers of "on" and "off" droplets in the group of droplets containing three or more beads. The solved q is then used to calculate λ following eq 1.

In the iddELISA assay, beads (diameter ~10 μm) are precoated with the capture antibody, and the analyte is mixed with the beads and the detection antibody, as shown in Figure

https://doi.org/10.1021/acs.analchem.4c04552
Anal. Chem. 2025, 97, 444−453

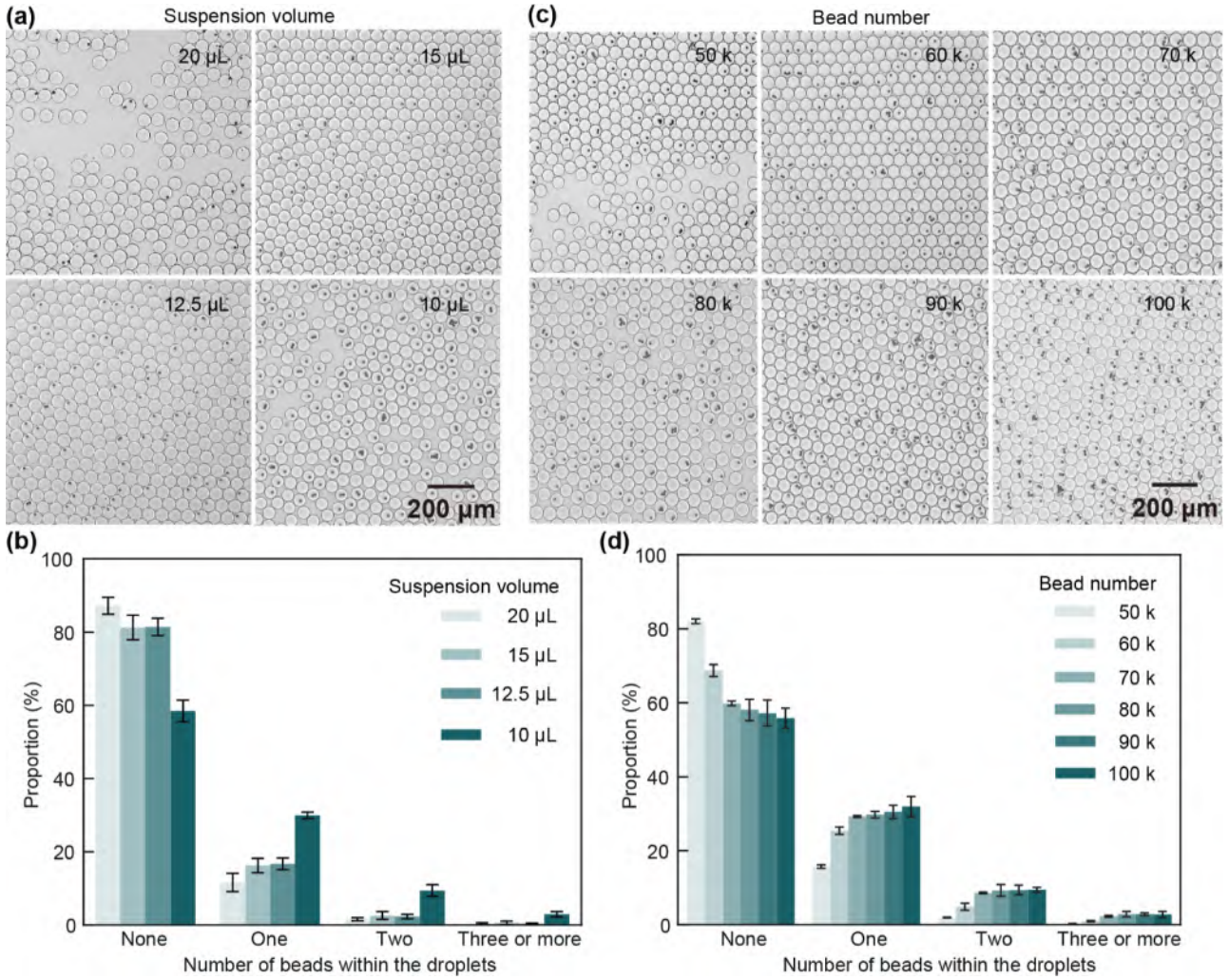

Figure 2. Effect of the bead density on the bead encapsulation. (a,b) Brightfield micrographs and quantified data showing the bead encapsulation within droplets using different suspension volumes. (c,d) Brightfield micrographs and quantified data showing the bead encapsulation within droplets using different numbers of beads. Error bars represent the standard deviations of three replicates.

1a. After incubation, the enzyme, e.g., horseradish peroxidase (HRP), is supplemented to complete the immuno complex via biotin−streptavidin binding. The beads are then collected and dispersed in droplets (diameter of 49.69 ± 1.50 μm) along with the HRP substrates in a microfluidic device (Figures 1b and S1) before being incubated and imaged. In the image analysis, droplets are segmented in the brightfield first, and the corresponding fluorescence images are analyzed to determine the "on"−"off" status. The beads are then detected to obtain the bead number within each droplet (Figure 1c). These two sets of data are tallied and used to solve for λ using eqs 6 and 1, which is used to calculate the analyte concentration based on the calibration curve.

The turnaround time of the iddELISA was approximately 70 min, including 40 min for the formation of immuno complex on beads, 10 min for subsequent washing, 15 min for droplet generation and imaging, and 5 min for data analysis.

Optimization of the Bead Encapsulation. We sought to optimize the bead encapsulation by looking into the microfluidic droplet generation. We started by optimizing the flow rates to ensure a stable droplet generation with desirable sizes. We kept the flow rates of the two aqueous phases containing the beads and substrate, respectively, equal and adjusted them while fixing the flow rate of the carrier oil to 1200 μL/h. The results indicated that flow rates of 240 μL/h allowed relatively robust generations of droplets with diameters of 49.69 ± 1.50 μm (Figure S2).

The bead density affects the Poisson encapsulation statistics and thereby the distribution of the bead numbers within the resultant droplets. After the formation of the immuno complexes on the beads, the beads are resuspended in solution for the subsequent encapsulation. Therefore, both the suspension volume and the bead number determine the bead density. We adjusted the suspension volume while keeping the bead number at 80k. The results showed that with a smaller suspension volume and thus higher bead density, there were fewer empty droplets and more droplets with multiple beads (Figure 2a). For example, when the liquid volume decreased from 20 to 10 μL, the proportion of empty droplets decreased from 86.67 ± 2.00% to 58.09 ± 2.40%, and the proportion of droplets containing two beads increased from 1.48 ± 0.40 to 9.31 ± 1.3% (Figure 2b). In principle, 10 μL suspension allows the formation of more than 300k droplets, which would be adequate for the subsequent analysis.

We then investigated the effect of bead numbers on the encapsulation by using different bead numbers while keeping

https://doi.org/10.1021/acs.analchem.4c04552
Anal. Chem. 2025, 97, 444−453

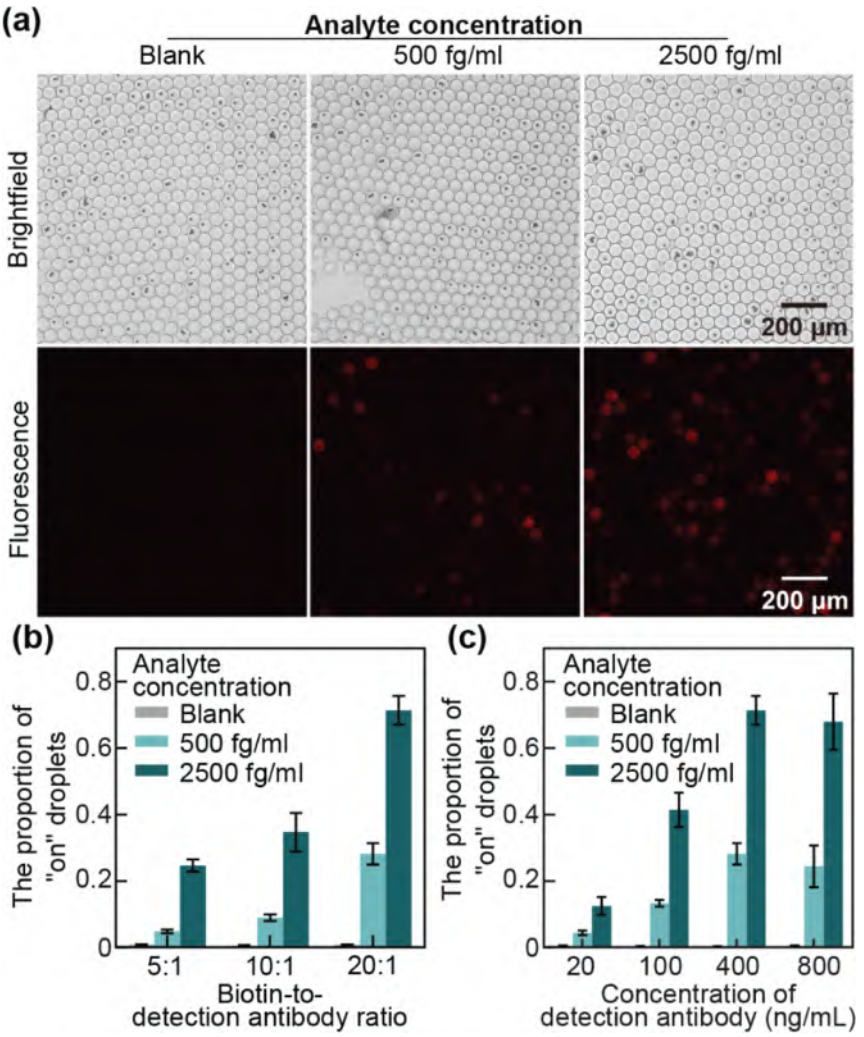

Figure 3. Optimization of the experimental conditions of the detection antibody. (a) Representative brightfield and fluorescence micrographs of the droplets after enzymatic reactions using a 20:1 biotin-to-detection antibody ratio and 400 ng/mL detection antibody concentration when testing samples with different analyte concentrations. (b) The proportion of "on" droplets in assays using different biotin-to-detection antibody ratios. (c) The proportion of "on" droplets in assays using different concentrations of detection antibody. Error bars represent the standard deviations of three replicates. The images of all experimental conditions for (b,c) were presented in Figures S4 and S5.

the suspension volume at 10 μL. As expected, higher bead numbers led to more frequent appearances of bead-loaded droplets (Figure 2c). For example, as the bead number increased from 50 to 80k, the proportion of empty droplets showed a substantial decrease from 82.04 ± 0.53% to 59.86 ± 0.50% (Figure 2d). However, after that, the increase in the bead number showed minimal effect on the encapsulation, and channel clogging happened occasionally. Therefore, the suspension volume of 10 μL and the bead number of 80k were chosen for the iddELISA assays.

Optimization of the Immunoreactions. We then sought to determine the optimal conditions regarding the immunoreactions. The N protein of the SARS-CoV-2 virus was selected as the detection target for the demonstration of assay performance, and the selected antibodies were validated by the supplier and in previous studies.[18−20]

Before the iddELISA assays, beads are precoated with the capture antibody. We first verified in bulk immunoassays that when 1.6 million beads were suspended in 50 μL solution, supplementing 40 μL capture antibody (7.35 mg/mL) could generate an adequate signal-to-noise ratio while being cost-effective (Figure S3). We then systematically investigated how the experimental conditions of the detection antibody affected the assay results. We first investigated the biotin-to-detection antibody ratio using ratios spanning the range recommended by the supplier, namely 5:1 to 20:1, and tested a range of analyte concentrations following the iddELISA assay processes. The results showed that these biotinylation conditions enabled a progressive increase in the proportion of "on" droplets as the analyte concentrations increased (Figure S4). In particular, with a biotin-to-detection antibody ratio of 20:1, the proportion of "on" droplets showed the most dramatic change as the analyte concentration increased (Figure 3a,b). The proportion of the "on" droplets at this ratio was 0.81 ± 0.08%, 28.17 ± 2.65%, and 71.40 ± 3.54% when the analyte concentration was 0, 500, and 2500 fg/mL, respectively, implying a higher sensitivity compared to the experiments using smaller ratios. We further studied how the concentration of the detection antibody affected the assay results. Detection antibodies with concentrations of 20, 100, 400, and 800 ng/mL were incubated with analytes of different concentrations. The results showed that the proportion of "on" droplets

https://doi.org/10.1021/acs.analchem.4c04552
Anal. Chem. 2025, 97, 444−453

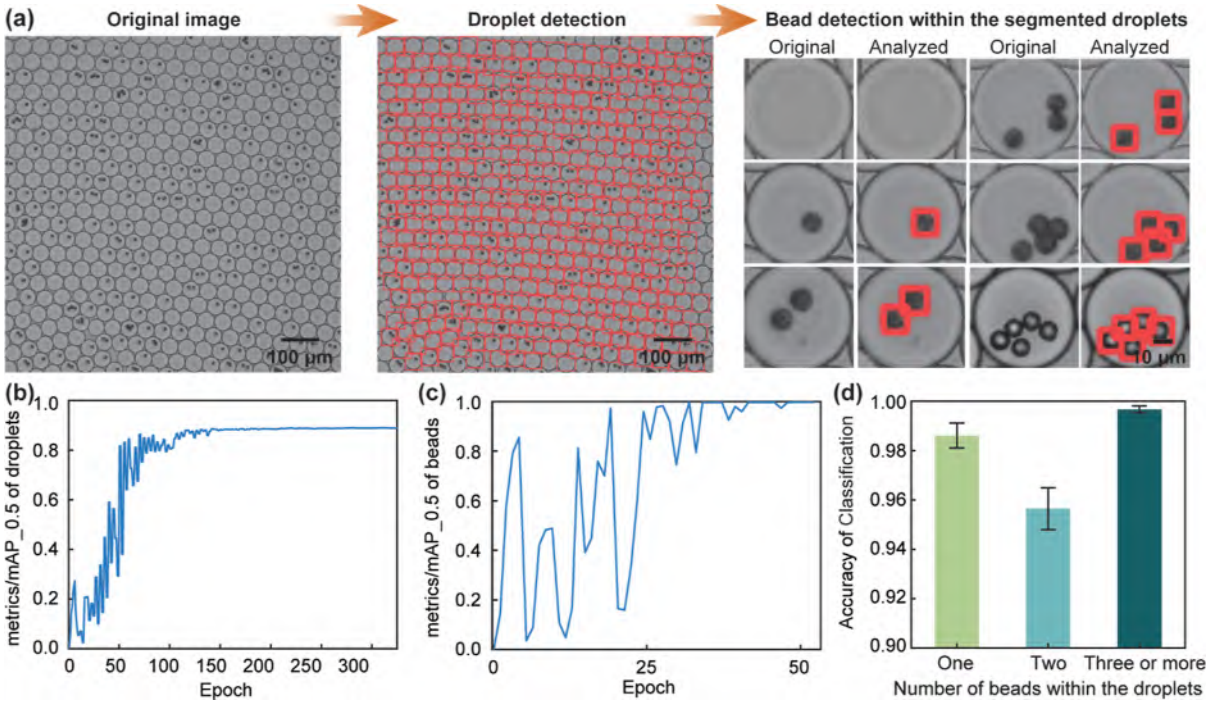

Figure 4. Image analysis pipeline and performance characterization. (a) The flowchart of the image analysis pipeline. Droplets were detected first before the beads were detected within each droplet. Both object detection tasks used the deep learning algorithm of YOLOv5 (b,c) mean average precision (mAP) as a function of epochs for the droplet and bead detection. (d) The classification accuracy of the analyzed droplets encapsulating different numbers of beads in subsequent experiments. The accuracy of all types of droplets was higher than 0.95. Error bars represent the standard deviations of three replicates.

increased with higher analyte concentrations (Figures 3a and S5). In addition, the proportion of "on" droplets also increased as a more concentrated detection antibody solution was applied. After the concentration reached 400 ng/mL, little change in the proportion of "on" droplets was observed, presumably because the detection antibody had become overloaded (Figure 3c). Therefore, the 20:1 biotin-to-detection antibody ratio was adopted for biotinylating, and the 400 ng/mL detection antibody concentration was used in the assay.

We additionally optimized the choice of the streptavidin labeled enzyme, namely plain horseradish peroxidase (HRP), high sensitivity HRP (HS-HRP), and polymerized form of HRP (poly-HRP). The enzyme solutions were mixed with the substrate (Amplite red) in a Y-shaped microfluidic channel and then emulsified immediately by the carrier oil. The droplets were then incubated and imaged to assess the fluorescence intensity. The results showed that HS-HRP had high enzymatic activity on the substrate and generated bright fluorescence within 10 min, which was suitable for the experimental operation and imaging process (Figure S6). Therefore, HS-HRP conjugated with streptavidin was chosen for the iddELISA assay.

Deep Learning-Based Image Analysis. With the bead encapsulation and immunoreaction protocols established, we aimed to develop the image analysis pipeline for droplet and bead detection. We adopted a two-step strategy: the objects of droplets were detected first and segmented, and the objects of beads were detected within the segmented droplets (Figure 4a). In addition, the "on"−"off" status of the droplets was analyzed in the fluorescence images by mapping the bounding boxes from the brightfield images. The analyzed bead number and "on"−"off" status of each droplet were used to tally the droplets for the AEB calculation.

Both object detection tasks were implemented using the deep learning algorithm of YOLOv5 owing to its demonstrated performance in such tasks.[21,22] The data sets for droplet recognition were obtained by labeling approximately 27 thousand droplets in 60 brightfield micrographs. The ratio of training and test data sets was set at 2:1. As expected, the implemented model achieved good detection performance. The mean Average Precision (mAP) at the Intersection over the Union (IoU) threshold of 0.5 (mAP@0.5) reached a stable level at around 0.89 after 100 epochs in the training (Figure 4b). The false positives included incomplete droplets straddling the image boundaries with skewed aspect ratios, which were excluded in the post processing. The detection of beads was relatively more straight forward, given their easily distinguishable size and morphologies. Therefore, the data set included only 500 labeled beads, and a similar training strategy was adopted. Consequently, the mAP@0.5 approached 1 after only 40 epochs (Figure 4c).

In typical experiments of iddELISA assays, 100 brightfield micrographs were captured and analyzed by the algorithm, which detected 20−25 thousand droplets and 10−15 thousand beads for subsequent data processing. The classification accuracy for droplets containing one, two, and three or more beads was 98.61 ± 0.50%, 95.65 ± 0.85%, and 99.66 ± 0.14%, respectively, as confirmed by manual inspection (Figure 4d). The overall data processing took less than 5 min.

Characterization of the Analytical Performance of the iddELISA. We then performed the complete assays of the iddELISA using samples with analyte concentrations ranging from 2 to 12,500 fg/mL (0.045 to 278 fM). In the analysis of the "on"−"off" status based on the droplet fluorescence, the

https://doi.org/10.1021/acs.analchem.4c04552
Anal. Chem. 2025, 97, 444−453

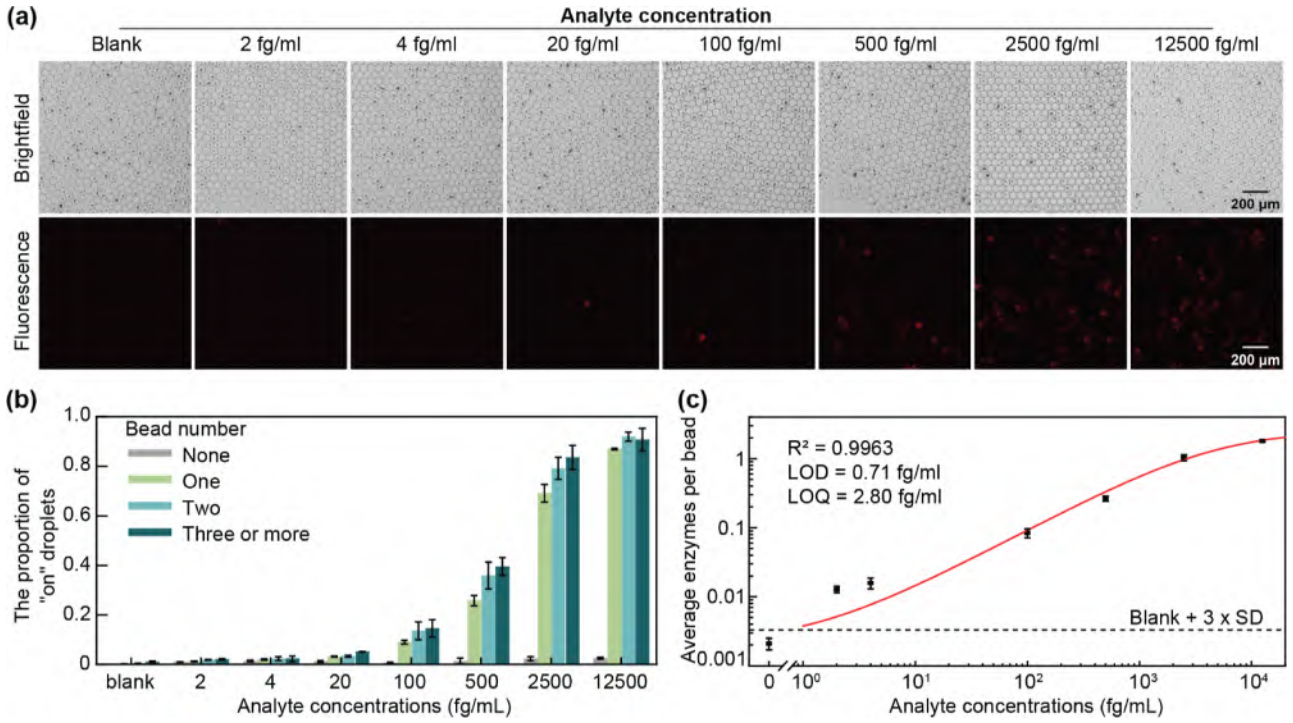

Figure 5. Characterization of the analytical performance of the iddELISA. (a) Brightfield and fluorescence micrographs of droplets after the iddELISA when testing samples with different analyte concentrations. (b) The proportion of "on" droplets among different droplet encapsulation groups when testing samples with different analyte concentrations. (c) Fitting the calculated average enzymes per bead at different analyte concentrations into a logistic curve. Error bars represent the standard deviations of three replicates.

cutoff threshold was defined as the mean fluorescence intensity of droplets containing no bead plus 5 standard deviations in each experiment. This internally defined cutoff threshold reduced the experiment-to-experiment variations in the fluorescence intensity. Consequently, the incidence of false positives among the droplets containing no bead remained minimal in different experiment groups.

The results showed the iddELISA could indeed capture the gradual increase in the analyte concentrations. As shown in Figure 5a,b, as the analyte concentrations increased, the proportion of "on" droplets gradually increased as a whole. For example, at the analyte concentration of 4 fg/mL, the proportion of "on" droplets among the droplets containing beads was 2.21 ± 0.16%; at 2500 fg/mL, the proportion was 77.30 ± 6.07%. In addition, droplets containing more beads generally exhibited higher chances of being "on" droplets. For example, at the analyte concentration of 2500 fg/mL, the proportion of "on" droplets among the droplets containing one, two, and three or more beads were 69.12 ± 3.54%, 79.15 ± 4.46%, and 83.64 ± 4.81%, respectively, showing an upward trend. The specific values did not perfectly agree with the prediction by eq 2, which used observed value of 69.12% to predict proportions of 90.46% and 97.06% for droplets containing two and three or more beads, respectively. This discrepancy was likely because the beads occasionally aggregated during the processing (e.g., Figure 2a,c), which reduced the total available surface areas and thus the chance of containing at least one enzyme.

The data were used to calculate the AEB values, which were then used to fit a four-parameter logistic curve as common practice for the calibration of digital ELISA assays.[23] The AEB values showed a good agreement with the regression model (R^2 = 0.99). The iddELISA assay with the optimized assay conditions also showed good analytical performance, with the limit of detection (LOD) being 0.71 fg/mL (15.78 aM) and the limit of quantification (LOQ) being 2.80 fg/mL (62.22 aM), as calculated by the mean AEB value of blank controls plus 3 and 10 standard deviations, respectively. To benchmark the performance of iddELISA, we performed both conventional ELISA and standard ddELISA using the same set of reagents. The results showed that conventional ELISA had a LOD of 4.12 pg/mL, which was much higher than that of the iddELISA (Figure S7). The experiments of standard ddELISA showed a LOD of 7.01 fg/mL, which was also higher than iddELISA (Figure S8). These results confirmed the enhanced capability of the iddELISA in the detection of low concentrations.

To evaluate the repeatability of the iddELISA, we performed additional tests, calculated the AEBs using the algorithms, and calculated the concentrations using the calibration curve. The concentrations, namely 20, 100, and 2500 fg/mL, were chosen to represent different concentration spots. As shown in Figure 6, the measurements showed good accuracy, with recovery rates ranging from 91.80% to 109.38%. In addition, the coefficients of variation at all test concentrations were less than 13%. These results suggested that the iddELISA assays had relatively good repeatability.

To evaluate the specificity of the iddELISA, we tested samples containing the N protein of MERS-CoV at a high concentration (1 ng/mL) due to its structural similarity to SARS-CoV-2 N protein. The measured AEBs were 0.0074 ± 0.0029, moderately higher than those from the blank samples (AEB: 0.0021 ± 0.0004). However, these values were still lower than the AEBs obtained from testing 2 fg/mL of SARS-CoV-2 N protein, which had AEBs in the range of 0.013 ± 0.001 (Figure 5c inset). These results confirm the good

https://doi.org/10.1021/acs.analchem.4c04552
Anal. Chem. 2025, 97, 444−453

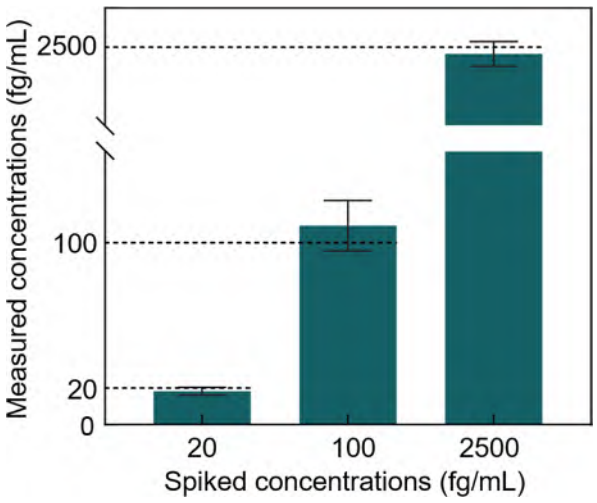

Figure 6. Validation of the iddELISA assay using spiked samples with different concentrations as indicated. Errors represent standard deviations from 6 replicates.

specificity of iddELISA. The specificity was further validated by testing analytes spiked in a 10% artificial saliva matrix, where iddELISA achieved a LOD of 1.26 fg/mL, demonstrating its capability to detect analytes in biologically relevant backgrounds (Figure S9).

DISCUSSION AND CONCLUSIONS

In this study, we report a new concept of digital ELISA, named iddELISA, which includes droplets encapsulating multiple beads in the analysis. We derived the model for the statistical inference of the average enzymes per bead, systematically optimized the bead encapsulation and the immunoreactions, and developed the image analysis pipeline for accurate detection of the droplets and beads, before testing the analytical performance of the iddELISA assays. The iddELISA demonstrated simplified operation, improved counting efficiency, and enhanced capability compared to standard ddELISA.

The improvement over standard ddELISA is likely due to the inclusion of droplets containing multiple beads in the analysis. For instance, assuming the average number of enzymes per bead is 0.01, in standard ddELISA, the proportion of "on" droplets among all nonempty droplets would be 1%, as calculated using eq 2 with $i = 1$. However, in iddELISA, where i can be greater than 1 in eq 2, the proportion of "on" droplets would be 1%, 1.99%, and 2.97% among droplets containing one, two, and three beads, respectively. This leads to an overall proportion of "on" droplets greater than 1%. Consequently, with the same detection resolution for "on" droplets, iddELISA can detect lower analyte concentrations than standard ddELISA, resulting in a lower LOD. In fact, we extracted the droplets containing single bead within the iddELISA data set and analyzed the analytical performance. The results indicated a LOD of 1.21 fg/mL, which was higher than the 0.71 fg/mL achieved with the full iddELISA (Figure S10), highlighting the advantage of including droplets with multiple bead encapsulations in the analysis.

The current form of iddELISA is primarily optimized for digital detection at low analyte concentrations. At higher concentrations, where the average number of enzymes per bead increases, the theoretical proportion of "on" droplets (as predicted by eq 2) should be higher than in ddELISA, potentially reducing detection sensitivity. To better understand the impact of multiplet-bead encapsulation on the increase of "on" droplets, we calculated the proportions of "on" droplets among nonempty droplets at varying bead densities and analyte concentrations, based on the Poisson distribution. Bead densities were represented by the average number of beads per droplet, ranging from 0.1 to 3.0, and analyte concentrations were represented by the average number of enzymes per bead, ranging from 0.01 to 2.0. The results indicated that higher average beads per droplet indeed lead to faster saturation (Figure S11). For instance, when the average beads per droplet was 3.0, the proportion of "on" droplets reached 0.8 at an AEB of approximately 0.7. In contrast, with an average beads per droplet lower than 0.5, the proportion of "on" droplets did not reach 0.8 until the AEB approached 1.5. These findings suggest that while the inclusion of multiple-bead encapsulation can enhance sensitivity at low concentrations, it also reduces the dynamic range at higher concentrations, which is a potential limitation of iddELISA.

Another limitation is that the current form of iddELISA does not support multiplex detection. In standard ddELISA, multiplex detection is typically achieved by coding antibody-coated beads with fluorescent dyes, a strategy that cannot be implemented in iddELISA due to the presence of multiple-bead encapsulation. Despite these potential limitations, iddELISA relaxes the stringent requirement for single-bead encapsulation and improves the detection limit, making the assay easier to implement. We envision that iddELISA will be particularly useful for detecting low-abundance biomarkers.

ASSOCIATED CONTENT

Data Availability Statement

All study data and material information are included in the article and SI Appendix. The image analysis software is available upon request.

Supporting Information

The Supporting Information is available free of charge at https://pubs.acs.org/doi/10.1021/acs.analchem.4c04552.

Additional experimental details, materials, and methods, including derivation of the statistical model, optimization of conjugation parameters, calibration curves, numerical analysis, and photographs of experimental setup (PDF)

AUTHOR INFORMATION

Corresponding Author

Zida Li − *School of Biomedical Engineering, Shenzhen University Medical School, Shenzhen University, Shenzhen 518060, China; Guangdong Key Laboratory of Biomedical Measurements and Ultrasound Imaging, School of Biomedical Engineering, Shenzhen University Medical School, Shenzhen University, Shenzhen 518060, China;* orcid.org/0000-0002-1353-9414; Email: zidali@szu.edu.cn

Authors

Yujuan Chai − *School of Biomedical Engineering, Shenzhen University Medical School, Shenzhen University, Shenzhen 518060, China; Guangdong Key Laboratory of Biomedical Measurements and Ultrasound Imaging, School of Biomedical Engineering, Shenzhen University Medical School, Shenzhen University, Shenzhen 518060, China*

https://doi.org/10.1021/acs.analchem.4c04552
Anal. Chem. 2025, 97, 444−453

Xiaoxiang Hu − *School of Biomedical Engineering, Shenzhen University Medical School, Shenzhen University, Shenzhen 518060, China*
Qi Fang − *School of Biomedical Engineering, Shenzhen University Medical School, Shenzhen University, Shenzhen 518060, China*
Yuanyuan Guo − *School of Biomedical Engineering, Shenzhen University Medical School, Shenzhen University, Shenzhen 518060, China*
Binmao Zhang − *School of Biomedical Engineering, Shenzhen University Medical School, Shenzhen University, Shenzhen 518060, China*
Hangjia Tu − *School of Biomedical Engineering, Shenzhen University Medical School, Shenzhen University, Shenzhen 518060, China*

Complete contact information is available at: https://pubs.acs.org/10.1021/acs.analchem.4c04552

Author Contributions

Yujuan Chai and Zida Li designed the research; Yujuan Chai, Xiaoxiang Hu, Qi Fang, and Yuanyuan Guo performed research; Yujuan Chai, Xiaoxiang Hu, Qi Fang, Yuanyuan Guo, Binmao Zhang, Hangjia Tu, and Zida Li analyzed data; Yujuan Chai, Xiaoxiang Hu, Qi Fang, and Zida Li wrote the paper.

Notes

The authors declare no competing financial interest.

■ ACKNOWLEDGMENTS

The authors thank Prof. Wenwen Chen from Shenzhen University and Dr. Siyi Hu from Suzhou Institute of Biomedical Engineering and Technology for insightful discussions on assay optimization. This research was funded by the National Natural Science Foundation of China (no. 22304121), Foundation for Distinguished Young Talents in Higher Education of Guangdong Province (no. 2022KQNCX067), University Innovation Team Project of Guangdong Province (no. 2021WCXTD002), Shenzhen Basic Research Project of Natural Science Foundation (no. JCYJ20230808105701004), Shenzhen Medical Research Fund (no. D2401011), and Medicine Plus Program of Shenzhen University (no. 2024YG015).

■ REFERENCES

(1) Li, Z.; Shum, H. C. Nanotechnology and Microfluidics for Biosensing and Biophysical Property Assessment: Implications for Next-Generation in Vitro Diagnostics. *Nanotechnology and Microfluidics*; Wiley, 2020; pp 83−107.
(2) Deng, J.; Ji, Y.; Zhu, F.; Liu, L.; Li, L.; Bai, X.; Li, H.; Liu, X.; Luo, Y.; Lin, B.; Lu, Y. *Proc. Natl. Acad. Sci. U.S.A.* **2022**, *119* (44), No. e2200944119.
(3) Chen, L.; Zhang, G.; Liu, L.; Li, Z. *Talanta* **2021**, *225*, 121986.
(4) Gao, Z.; Song, Y.; Hsiao, T. Y.; He, J.; Wang, C.; Shen, J.; MacLachlan, A.; Dai, S.; Singer, B. H.; Kurabayashi, K.; Chen, P. *ACS Nano* **2021**, *15* (11), 18023−18036.
(5) Jing, W.; Wang, Y.; Yang, Y.; Wang, Y.; Ma, G.; Wang, S.; Tao, N. *ACS Nano* **2019**, *13* (8), 8609−8617.
(6) He, L.; Tessier, D. R.; Briggs, K.; Tsangaris, M.; Charron, M.; McConnell, E. M.; Lomovtsev, D.; Tabard-Cossa, V. *Nat. Commun.* **2021**, *12* (1), 5348.
(7) Duffy, D. C. *Lab Chip* **2023**, *23* (5), 818−847.
(8) Rissin, D. M.; Kan, C. W.; Campbell, T. G.; Howes, S. C.; Fournier, D. R.; Song, L.; Piech, T.; Patel, P. P.; Chang, L.; Rivnak, A. J.; et al. *Nat. Biotechnol.* **2010**, *28* (6), 595−599.
(9) Song, Y.; Ye, Y.; Su, S.-H.; Stephens, A.; Cai, T.; Chung, M.-T.; Han, M. K.; Newstead, M. W.; Yessayan, L.; Frame, D.; et al. *Lab Chip* **2021**, *21* (2), 331−343.
(10) Kan, C. W.; Tobos, C. I.; Rissin, D. M.; Wiener, A. D.; Meyer, R. E.; Svancara, D. M.; Comperchio, A.; Warwick, C.; Millington, R.; Collier, N.; Duffy, D. C. *Lab Chip* **2020**, *20* (12), 2122−2135.
(11) Shim, J.-u.; Ranasinghe, R. T.; Smith, C. A.; Ibrahim, S. M.; Hollfelder, F.; Huck, W. T. S.; Klenerman, D.; Abell, C. *ACS Nano* **2013**, *7* (7), 5955−5964.
(12) Yelleswarapu, V.; Buser, J. R.; Haber, M.; Baron, J.; Inapuri, E.; Issadore, D. *Proc. Natl. Acad. Sci. U.S.A.* **2019**, *116* (10), 4489−4495.
(13) Li, L.; Wu, P.; Luo, Z.; Wang, L.; Ding, W.; Wu, T.; Chen, J.; He, J.; He, Y.; Wang, H.; et al. *ACS Sensors* **2019**, *4* (5), 1299−1305.
(14) Yue, X.; Fang, X.; Sun, T.; Yi, J.; Kuang, X.; Guo, Q.; Wang, Y.; Gu, H.; Xu, H. *Biosens. Bioelectron.* **2022**, *211*, 114384.
(15) Chen, L.; Zhao, Y.; Li, J.; Xiong, C.; Xu, Y.; Tang, C.; Zhang, R.; Zhang, J.; Mi, X.; Liu, Y. *Anal. Chem.* **2023**, *95* (23), 8889−8897.
(16) Yen, G. S.; Fujimoto, B. S.; Schneider, T.; Kreutz, J. E.; Chiu, D. T. *J. Am. Chem. Soc.* **2019**, *141* (4), 1515−1525.
(17) Chen, L.; Ding, J.; Yuan, H.; Chen, C.; Li, Z. *Adv. Sci.* **2022**, *9* (9), 2105450.
(18) Hryniewicz, B. M.; Volpe, J.; Bach-Toledo, L.; Kurpel, K. C.; Deller, A. E.; Soares, A. L.; Nardin, J. M.; Marchesi, L. F.; Simas, F. F.; Oliveira, C. C.; et al. *Mater. Today Chem.* **2022**, *24*, 100817.
(19) Miyamura, S.; Oe, R.; Nakahara, T.; Koresawa, H.; Okada, S.; Taue, S.; Tokizane, Y.; Minamikawa, T.; Yano, T.-A.; Otsuka, K.; et al. *Sci. Rep.* **2023**, *13* (1), 14541.
(20) Yasui, T.; Miyamura, S.; Oe, R.; Nakahara, T.; Okada, S.; Taue, S.; Tokizane, Y.; Minamikawa, T.; Yano, T.-a.; Otsuka, K. *Res Sq.* **2022**.
(21) Jocher, G. *YOLOv5 by Ultralytics Git code*, 2020. https://github.com/ultralytics/yolov5 (Accessed Nov 14, 2024).
(22) Wu, K.; Fang, Q.; Zhao, Z. T.; Li, Z. D. *Anal. Chem.* **2023**, *95* (11), 5069−5078.
(23) Brandmeier, J. C.; Jurga, N.; Grzyb, T.; Hlaváček, A.; Obořilová, R.; Skládal, P.; Farka, Z.; Gorris, H. H. *Anal. Chem.* **2023**, *95* (10), 4753−4759.
(24) Zeng, Y.; Gan, X.; Xu, Z.; Hu, X.; Hu, C.; Ma, H.; Tu, H.; Chai, B.; Yang, C.; Hu, S.; Chai, Y. *Anal. Chim. Acta* **2024**, *1298*, 342398.
(25) Erdem, A.; Senturk, H.; Yildiz, E.; Maral, M. *Talanta* **2022**, *244*, 123422.
(26) *Tzutalin. LabelImg. Git code*, 2015.